Available online at www.sciencedirect.com

ScienceDirect

IFAC PapersOnline CONFERENCE PAPER ARCHIVE

IFAC PapersOnLine 56-2 (2023) 8302–8307

Land/ocean absorption dynamics and airborne projection of carbon dioxide under finite fossil-fuel reserves

Carlo Novara*, Daniele Mazza, Enrico Canuto*****

**Politecnico di Torino, Dipartimento di Elettronica e Telecomunicazioni Torino, Italy (Tel: +39 011 0907019; e-mail: carlo.novara@polito.it).*
***Politecnico di Torino, Former Faculty (e-mail:mazzad50@gmail.com)*
****Politecnico di Torino, Former Faculty (e-mail:enrico.canuto@formerfaculty.polito.it)*

Abstract: The paper has been suggested by a pair of observations: 1) the atmospheric growth rate of carbon dioxide is smaller than that ascribed to the emission by fossil fuel combustion; 2) the fossil-fuel reserves are finite. The first observation leads to a simple dynamic model, based on the balance between the land-ocean absorption and the anthropogenic emissions of CO_2, only limited by the depletion of fossil-fuel reserves. The second observation suggests of projecting the historical CO_2 emissions in the future, by constraining them to the limit of reserve availability. Similar projections are available in the literature, but either driven by heuristics or by complex simulation packages. Here we provide a transparent and formal method only driven by historical data, their uncertainty and simple models. The method is proven capable of providing emission and concentration projections, which being constrained by finite reserves, may be taken as realistic bounds to forecasting exercises. The dynamics of the land-ocean absorption is proved by simplifying a more complex set of equations describing the CO_2 exchange between Earth's reservoirs. The contribution of other greenhouse gases like methane and nitrous oxide is neglected, as their emissions cannot be projected with the paper method. Notwithstanding this limitation, the paper results demonstrate that some of the IPCC projections are overestimated if compared to fossil-fuel physical limits, in agreement with other authors.

Keywords: carbon dioxide, fossil fuel, CO_2 absorption dynamics, finite reserve, future projection

1. INTRODUCTION

Future greenhouse gas (GHG), and especially carbon dioxide (CO_2) emissions by fossil fuel combustion, are the subject of extensive research, in relationships with the international pledges about net zero 2050 emissions (IPCC, 2022). The Intergovernmental Panel on Climate Change (IPCC) has developed long-term emission scenarios up to 2100 (Houghton et al, 1990). These scenarios have been used in the analysis of possible climate change due to increase of atmospheric GHG concentration and options for mitigating the change. Scenarios and simulations (see Eyring et al., 2016) do not explicitly mention, as a limiting factor of the fossil fuel emissions, their physical reserves.

The topic of 'fossil fuel resources (here *reserves*) as a constraint in emissions scenarios' is dealt with by Vernon (2011). Other authors like Welsby et al. (2021) treat the topic for predicting the unextracted reserves under IPCC mitigation strategies. Distinction must be done between reserves and resources (Bebbington et al., 2020). Resource is that amount of a natural commodity that exists in both discovered and undiscovered deposits. 'Reserves', to be addressed here, are the subgroup of a resource that have been discovered, have known size, and can be recovered.

The goal and novelty of this paper is to offer a complete, formal and statistically proven procedure for converting historical CO_2 concentration and emission data into a simple dynamic model that allows measurements to be projected into the future, while respecting the constraint of finite fossil-fuel reserves. The paper starts from the CO_2 concentration as measured by the Mauna Loa observatory since 1958 (the Keeling curve, see SCRIPPS CO_2 program, 2022), thus neglecting other atmospheric GHGs like methane and nitrous oxide as they depend on different emission sources and removal mechanisms (Peng et al, 2022). CO_2 is dynamically exchanged among atmosphere, biomass, land and ocean as in Archer (2010). A big deal of carbon dioxide is taken out from atmosphere by photosynthesis, but at the same time, half of this goes back to air by plant emission and animal breathing. Part of the remainder goes to soil after plant death and, due to bacterial fermentation, again into the air. Estimates performed by computerized models have been collected by the Global Carbon Project (GCP, Friedlingstein, 2022).

Before industrial era, ice-core data of the last 2000 years show the airborne CO_2 concentration fluctuating around $\underline{x} = 280 \pm 10$ ppm (*historical equilibrium*), then since the XIX century slowly growing until World War II and then steadily increasing. As a result, the periodic annual exchange between land, ocean and atmosphere is accompanied by an atmospheric increase, small if compared with the annual exchange, but progressively accumulating.

Actually, things look not so simple, since the annual emission happens to be larger than the corresponding air concentration growth, implying that part of the accumulated

10.1016/j.ifacol.2023.10.1018

CO_2 is absorbed by soil and ocean as they behave as carbon sinks. Fig. 1 shows the cumulative fossil fuel emission since 1750 (blue line) and the airborne CO_2 concentration [ppm] (red line) above the historical equilibrium $\underline{x}$. Effects of ocean CO_2 absorption, like increase of hydrogen ion concentration (acidification, Archer, 2010), are not topics of the paper.

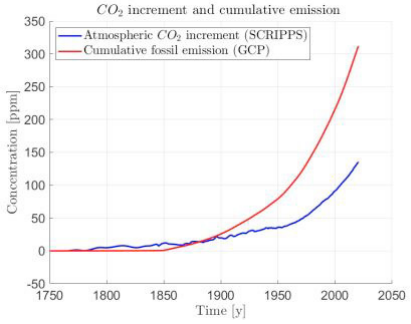

Fig. 1. Industrial era: airborne CO_2 concentration increment and cumulative fossil fuel emission.

A question concerns how long a perturbation of the airborne CO_2 takes to be absorbed by soil and ocean sinks. An answer will be given in Section 2, aiming to forecast the airborne concentration based on an appropriate dynamic model. The absorption time constant should not be confused, as pointed out by Archer (2010), with the residence time of the annual land/ocean-atmosphere two-way, zero-mean flow. The latter is the CO_2 transport delay in the atmosphere. The absorption time constant is elongated by the so-called carbon feedback (Archer, 2010, Friedlinsgtein et al. 2003). Absorption weakens with increasing temperature, which latter in turn increases with the airborne carbon concentration.

Several packages have been developed by studies of global climate prediction. Here, a simple dynamic model of the CO_2 absorption is derived, mimicking the chemical kinetics of the exchange between atmosphere and land/ocean. The model results from simplifying a set of state equations, where each state variable accounts for the carbon amount of the Earth's reservoirs, including fossil fuel deposits. Model simplification leads to a first-order state equation with two unknown parameters: (i) the equilibrium concentration of the airborne CO_2, close to the mean value of the last two millennia, (ii) the land/ocean absorption time constant, close to half a century. Data uncertainty reflects onto parameter variance, which allows predictions with statistical bounds.

Based on the Section 2 model, historical data of the fossil fuel depletion are predicted in Section 3 with the help of the Meixner distribution, a typical logistic curve, constrained by current reserves. The predicted depletion, converted into equivalent CO_2 emission, becomes the input of the absorption dynamic model. Starting from the current epoch, the model integrates the predicted emissions, decremented by land and ocean absorption, thus providing finite-reserve projections of the airborne CO_2 concentration until $t_{End} = 2150$. The last term has been delayed since the usual 2100 term for accommodating a realistic depletion of the large coal reserves.

Section 4 includes a preliminary comparison with the projections of the IPCC simulations packages driven by business-as-usual and mitigation policies (IPCC, 2021). Only part of the projections complies with the paper finite-reserve predictions as already observed by other authors. The paper closes with a brief discussion and analysis, which takes advantage of the dynamic model in Section 2.

2. DYNAMICS OF LAND/OCEAN ABSORPTION

2.1. State equations of CO_2 reservoirs

The aim is to formulate a dynamic model of the annual mean carbon evolution, which excludes the zero-mean seasonal perturbations, but is capable of fitting the airborne carbon drift of the industrial era. It seems natural to formulate atmosphere ($s = 1$), ocean ($s = 2$), land ($s = 3$), cement constructions ($s = 4$) and fossil fuel deposits ($s = 5$) as separate *reservoirs* capable of storing a carbon amount x_s . The state variables are collected into the column vector $\boldsymbol{x} = [x_1, x_2, x_3, x_4, x_5]$, where an inline notation has been adopted. The term reservoir implies both emission and uptake, whereas sink just indicates uptake and deposit emission. The unit of x_s is the CO_2 mass in billions of metric tons [$GtCO_2$], but the equivalent part per million of moles of dry air [ppm] will be also used, under the equivalence 1 ppm=7.82 $GtCO_2$.

The time rate of $x_s(t)$ is a combination of input flows $v_{hs}(x_h, \Theta) > 0$ from other reservoirs, output flows $-v_{sh}(x_s, \Theta)$ and the anthropogenic flow $b_h u_h$, as follows:

$$\dot{x}_s(t) = \sum_{h\neq s}\big(-v_{sh}(x_s, \Theta) + v_{hs}(x_h, \Theta) + b_h u_h(t)\big), \qquad (1)$$

where Θ is the boundary temperature, $b_h = \{-1,0,1\}$ and $x_s(t_0) = x_{s0}$. Equation (1) specializes into (i) the atmospheric equation, $s = 1$, with $b_h = 1$ (all the reservoirs contribute to the airborne CO_2) and $v_{15} = v_{51} = 0$, (ii) the fossil-fuel equation $\dot{x}_5(t) = -u_5(t)$, $x_5(t_0) = x_{50}$, and (iii) the ocean, land and cement equation

$$\dot{x}_s(t) = -v_{s1}(x_s, \Theta) + v_{1s}(x_1, \Theta) - u_s(t), \qquad (2)$$

where $x_s(t_0) = x_{s0}$, $s = 2,3,4$, the input flow v_{1s} comes only from atmosphere (uptake), and the output flows (emissions) are the natural $-v_{s1}$ and anthropogenic flow $-u_s$. The exchange flows $v_{sh}, v_{hs}, h \neq 1$ have been neglected in (2). The most significant is the land-to-ocean flow v_{32}, which from Regnier et al. (2022) can be estimated between 5% and 15% of the airborne CO_2 growth. The flow becomes an internal flow, if land and ocean are treated as a single sink.

A simple result is that the overall Earth's CO_2 amount $x_0 = \sum_s x_s(t)$ is constant, having neglected the contribution of volcanic eruptions. A pair of equilibria (underlined symbols) are arbitrary, for instance $\{\underline{x}_0, \underline{x}_5\}$, which looks reasonable as they cannot be fixed by exchanges. By substituting $\underline{x}_0$ with the airborne historical equilibrium $\underline{x}_1 = 280$ ppm, the land, ocean and cement equilibria, denoted by $\underline{x}_s, s = 2,3,4$, follow from the identity $v_{s1}(\underline{x}_s, \underline{\Theta}) = v_{1s}(\underline{x}_1, \underline{\Theta})$, $\underline{\Theta}$ being the equilibrium temperature.

We are interested in the recent Holocene equilibrium perturbation, like that of the airborne $\delta x_1 = x_1 - \underline{x}_1$ and of the temperature $\delta\Theta = \Theta - \underline{\Theta}$, due to anthropogenic emissions. By replacing, in (1), the first-order expansion

$$v_{sh}(x_s, \Theta) = v_{sh}(\underline{x}_s, \underline{\Theta}) + k_{sh}\,\delta x_s(t) + g_{sh}\delta\Theta(t), \qquad (3)$$

and by taking into account the previous specializations, the following linear system of equations is obtained

$$\delta\dot{\boldsymbol{x}}(t) = A\delta\boldsymbol{x}(t) + B\boldsymbol{u}(t) + G\delta\Theta(t), \delta\boldsymbol{x}(t_0) = \delta\boldsymbol{x}_0. \quad (4)$$

Vectors and matrices are given by

$$\delta\boldsymbol{x} = [\delta x_1, \dots, \delta x_5], \qquad \boldsymbol{u} = [u_2, u_3, u_4, u_5] \quad (5)$$

and

$$A = \begin{bmatrix} -k_{12}-k_{13}-k_{14} & k_{21} & k_{31} & k_{41} & 0 \\ k_{12} & -k_{21} & 0 & 0 & 0 \\ k_{13} & 0 & -k_{31} & 0 & 0 \\ k_{14} & 0 & 0 & -k_{41} & 0 \\ 0 & 0 & 0 & 0 & 0 \end{bmatrix}$$
$$G = \begin{bmatrix} g_1 \\ g_2 \\ g_3 \\ g_4 \\ 0 \end{bmatrix}, B = \begin{bmatrix} 1 & 1 & 1 & 1 \\ -1 & 0 & 0 & 0 \\ 0 & -1 & 0 & 0 \\ 0 & 0 & -1 & 0 \\ 0 & 0 & 0 & -1 \end{bmatrix} \quad (6)$$

where the coefficients $g_{sh}, h \neq s$ of each equation have ben summed up into g_s. Any parameter k_{sh} in (6) has the meaning of a chemical kinetic constant as explained below.

The temperature perturbation dynamics in Mazza, Canuto and Novara (2022) can be converted into the identity

$$g_1\delta\Theta(t) = k_{CF}\delta x(t) + w(t), k_{CF} > 0, \quad (7)$$

where k_{CF} is the carbon feedback gain and $w(t)$ accounts for temperature fluctuations independent of δx.

In the paper, restricted to airborne carbon projection, the system (4) can be reduced to the first and last equations, under the assumption that during the regression and projection time interval from 1955 to 2150, x_s, $s = 2,3,4$, remains constant and equal to the equilibrium, namely $x_s = \underline{x}_s$. The assumption may appear incautious, but Mazza, Canuto and Novara (2022) proved that $x_s \cong \underline{x}_s$ corresponds to $\underline{x}_s \gg \underline{x}_1$, which is fairly true for $s = 2$ (ocean) and $s = 3$ (land). By dropping subscript 1, by setting $r = x_5$, $c = u_5$ and employing (7), the pair of equations can be rewritten as follows:

$$\begin{matrix} \dot{x}(t) = -k\big(x(t) - \underline{x}\big) + u(t) + w(t), x(t_0) = x_0 \\ \dot{r}(t) = -c(t), \qquad r\big(t_p\big) = R \end{matrix}. \quad (8)$$

In (8), by recalling the assumption $x_s = \underline{x}_s$, we have:

$$\begin{matrix} u = u_2 + u_3 + u_4 + u_5, \; k\underline{x} = \sum_{s=2,3,4} k_{s1}\underline{x}_s \\ k = k_{12} + k_{13} + k_{14} - k_{CF} = k_{abs} - k_{CF} > 0 \end{matrix}, \quad (9)$$

where carbon feedback is accounted for by $k_{CF} > 0$.

Of the components of u, $u_2 = u_4 = 0$, whereas the land-use change u_3 may be decomposed into mean and fluctuation as $u_3 = \underline{u}_3 + \tilde{u}_3$. The mean $\underline{u}_3$, which contributes to the equilibrium $\underline{x}$, may be employed as a prediction, but treating $\underline{x}$ as a total unknown is such to attenuate estimate uncertainty. The fluctuation $\tilde{u}_3$ is absorbed by the unpredictable $w(t)$. Thus, $u = u_5$ only accounts for fossil fuel emissions by combustion. Actually, GCP data (see Fig. 1) include production emissions, which stays within data uncertainty.

In (8), $t_p = 2021$ is the starting time of the projection, whereas $t_0 < t_p$ is the starting time of the raw data regression aiming to estimate the unknown pair $\{k, \underline{x}\}$. Finally, R denotes the ultimate fossil-fuel reserve that can be depleted. The state variable pair $\{x, r\}$ refers, in agreement with measurements, to the mean annual concentration from January to December. Raw data refer to the annual airborne concentration $\breve{x}(t_i) = x(t_i) + \tilde{x}(t_i)$ from Mauna Loa data and to the CO_2 emission $\breve{u}(t_i) = u(t_i) + \tilde{u}(t_i)$, where $t_i = iT$ and $T = 1$ y. The breve mark in $\breve{x}$ denotes measurements, tilde in $\tilde{x}$ denotes errors.

A similar equation to (8) can be found in Revelle at al. (1957), but restricted to ocean. Models in Tans (2009) and Connolly et al. (2020) include bounded-input-bounded-output unstable terms, unsuitable to long-term projections. Carbon cycle literature like Friedlingstein et at. (2003) and the subsequent, like Zhang et al. (2021), employ static perturbation equations.

2.2. Physical justification

References are Zeebe and Wolf-Glabrow (2001) and Mazza and Canuto. (2022). The main Earth's reservoirs capable of absorbing airborne CO_2 are ocean and land. Ocean absorption can be explained by seawater reactivity, alkaline in character. The reversible reactions taking place at the atmosphere-ocean boundary read as

$$CO_2(\text{gas}) + H_2O \;\Leftrightarrow\; CO_2(\text{aq}) + H_2O \;\Leftrightarrow\; H_2CO_3. \quad (10)$$

The direct reaction (left to right) describes the atmospheric CO_2 depletion and the reverse reaction (right to left) accounts for the oceanic CO_2 depletion. The land sink can be mainly explained by the photosynthesis, which encompasses, in the very first stages, a reaction similar to (10) between CO_2 and the water which constitutes the cell cytoplasm. Therefore, the concentration rate $d[CO_2]/dt$ of the airborne CO_2 can be written as the sum of the direct rate $v_{dir} = -k_{dir}[CO_2]$ (atmospheric depletion) and of the inverse rate $v_{inv} = k_{inv}[H_2CO_3]$ (atmospheric uptake) as follows:

$$\frac{d[CO_2](t)}{dt} = -k_{dir}[CO_2](t) + k_{inv}[H_2CO_3](t), \quad (11)$$

where square brackets denote concentration and the kinetic constants k_{dir}, k_{inv} $[y^{-1}]$ are assumed to be time-invariant. The inverse rate v_{inv} can be assumed as nearly constant due to slow variation of $[H_2CO_3]$ in the decade time span, which implies that the equilibrium of (11) holds $\underline{x} = \underline{[CO_2]} = v_{inv}/k_{dir}$. Equation (11) is only a part of the process, since every year an amount of anthropogenic CO_2, denoted as in (8) by $u(t)$, enters the atmosphere. Addition of u to (11), the identities $k = k_{dir}$, $x = [CO_2]$ and $k_{inv}[H_2CO_3] = k\underline{x}$, change (11) into (8) as expected.

2.3. Discretization and parameter estimation

By assuming $kT \ll 1$, the discrete-time version of (8) can be rewritten as the following difference regression equation:

$$\Delta\breve{x}(i) = -(1-a)\big(\breve{x}(i) - \underline{x}\big) + b(a)\breve{u}(i) + \Delta\tilde{x}(i), \quad (12)$$

where $\Delta\breve{x}(i) = \breve{x}(i+1) - \breve{x}(i)$ is the difference concentration measurement, $a = \exp(-kT)$, $b(a) = k^{-1}(1-a)$ and $\Delta\tilde{x}(i)$ is a nonstationary error including $w(t)$ of (8). Non-stationarity complies with the GCP raw data in Friedlingstein et al., 2022. The nonlinear least-squares (LS)

estimates of the difference regression (12) have been checked by the nonlinear LS estimates of the integral regression

$$\check{x}(i) = \underline{x} - a^i(\check{x}_0 - \underline{x}) + b\sum_{k=1}^{i} a^{i-k} k\, \check{u}(k-1) + \tilde{x}(i), \quad (13)$$

which is the sampled solution of (8). As a further check, the estimated difference $\Delta\hat{x}(i)$ of (12) was cumulated and compared with the Mauna Loa samples $\check{x}(i)$.

The residuals of the three regressions (difference=dark green, cumulative =cyan, integral= green) are overlapped in Fig. 2, together withe a priori (red) and a posteriori (blue) 3σ upper and lower bounds. Bounds increase due to the already mentioned non-stationarity.

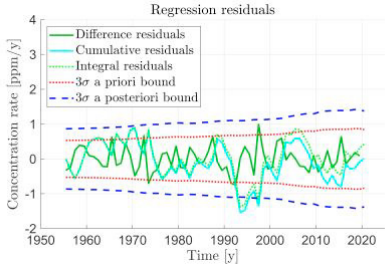

Fig. 2. Three kinds of regression residuals and their 3σ bands.

The integral estimate $\hat{x}(i)$ (dashed red), the raw data $\check{x}(i)$ (blue) and the estimated residuals $\tilde{x}(i)$ $(\times 10, \text{green})$, already in Fig. 2, are shown in Fig. 3. Raw data and the estimated profile are reported as increments from the estimated equilibrium (the zero dashed red line) in Table 1, third row.

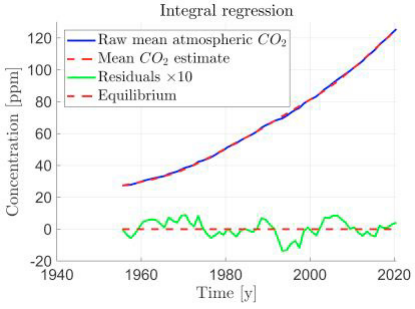

Fig. 3. Integral regression (the equilibrium is set to zero).

Table 1 reports the parameter estimates and their a posteriori standard deviation for the difference regression. Fairly the same values are provided by the integral regression. The complementary R-squared (ratio of the squared residual RMS and the total sum of squares), in log scale, proves the significance of model (8).

Table 1. Difference and integral regression results

No	Parameter	Symbol	Unit	Estim.	St.dev.
1	Kinetic constant	$\hat{k}$	1/y	0.0188	0.0015
2	Time constant	$\hat{\tau}$	y	53.1	4.3
3	Equilibrium	$\hat{\underline{x}}$	ppm	285.9	2.3
4	Historical equil.	$\hat{\underline{x}}_{hist}$	ppm	279.6	3.0
5	Integral regress.	$\log_{10}(1-R^2)$		−3.5	

Literature estimates are rather sparse. In Revelle at al. (1957), the estimate for the ocean absorption amounts to 10 y. In Archer (2010), a value of 100 y is reported. IPCC Working Group I reports values from 5 y to 200 y, by remarking that 'No single lifetime can be defined for CO_2 because of the different rates of uptake by different removal processes'. A confirmation of the $\hat{k}$ value in Table 1, row 1, can be deduced from Zhang et al., 2021, where the carbon feedback gain k_{CF}/k_{abs} (see (9)) has been estimated to about 2%

3. FORECASTING CO_2 CONCENTRATION

3.1. Fossil fuel emission model and projection

The second step is to employ (8) for forecasting the airborne concentration $x(t), t \geq t_p$, under the constraint of fossil-fuel finite reserves. We aim to forecast the emission $u(t), t \geq t_p$, which is assumed coincident with the total fossil-fuel emission $c(t) = \sum_{k=1}^{3} c_f(t)$ in (8), sum of the coal, oil and natural gas emissions $c_f, f = 1(\text{coal}), 2(\text{oil}), 3(\text{gas})$. The forecast of $c_f(t)$ is subjected to the integral constraint

$$\int_{t_p}^{t_{end}} c_f(\tau)d\tau = R_f,\ R = \sum_{k=1}^{3} R_f(t). \quad (14)$$

R_f is the estimated reserve and $c_f(t_{end}) = 0$ is assumed.

Let us consider a generic fuel, by dropping the subscript f except in R_f. Reserves have been projected from past data through the diminishing law

$$\frac{dm(t)}{m(t)} = -ns^{n-1}(t)ds(t),\ s(t) = \frac{t-t_0}{\tau}, t \geq t_0 \quad (15)$$

of the marginal reserve $m(t) = R_f - r(t)$, with initial value $m_0 = R_f - r_0$, and $1 < n < 2$ to account for increasing difficulties in converting resources into reserves (see Mazza, Canuto and Novara, 2022). The unknown parameters $\{m_0, R_f, \tau, n\}$ in (15) are found by fitting past reserve data.

Future emissions, in [$GtCO_2$] units, are predicted by a logistic model like the bell-shaped Meixner distribution:

$$c(t, \boldsymbol{p}) = \alpha \frac{\exp(\beta\, s(t))}{\cosh(s(t))},\ s(t) = \frac{t-\sigma}{\tau}. \quad (16)$$

Of $\boldsymbol{p} = [\alpha, \tau, \sigma, \beta]$, α is the height of the maximum for $\beta = 0$, τ defines the bell width, σ is the maximum abscissa for $\beta = 0$ and $-1 < \beta < 1$ is the skewness degree. The degree β tends to become unidentifiable when measurements are restricted to either lobe. This is the present case, forcing to assume $\beta = 0$. Nonetheless, paper projections agree with the literature as in Ward et al., 2011, and in the comparisons of Section 3.2.

Given the sequence $\check{c}_f(t_k), k = 0, \dots, N-1$, of emission measurements with $t_{N-1} = t_p$, and the reserve estimate R_f of the fossil fuel f, the regression equations are as follows:

$$\begin{aligned} \check{c}_f(t_k) &= g(t_k; \boldsymbol{p}_f) + \tilde{c}_f(t_k), k = 0, \dots, N-1 \\ R_f &= \sum_{k=N}^{N+M-1} g(t_k; \boldsymbol{p}_f) + \tilde{R}_f, f = 1,2,3 \\ 0 &= g(t_{end}; \boldsymbol{p}_f) + \tilde{c}_f(t_{end}) \end{aligned}, \quad (17)$$

where $t_{N+M-1} = t_{end}$. The first equation fits (16) to the fossil fuel data, the second is the discrete-time version of (14) and the last forces the end projection to zero. The regression criterion is a weighted sum of the square errors in (17).

The 3σ bands in Fig. 4 account for the a posteriori variance of the estimated reserve and of the parameter estimate $\hat{\boldsymbol{p}}$ in (16) from the historical emission data. The band around historical data, $t \leq t_p$, is smaller than around the projected profiles.

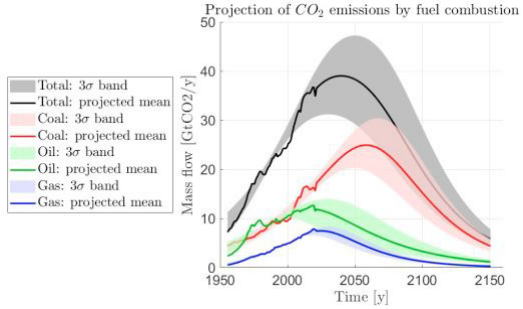

Fig. 4. Projections of the CO_2 emissions by fuel and their total profile together with their 3σ uncertainty bands (shaded areas).

3.2. Comparison with literature

Two sets of profiles have been selected for comparison: those of the Climate Action Tracker, CAT (2022, data are available) and those in IPCC (2021). Of the latter ones, we could not find data but only images in Lindsay (2022).

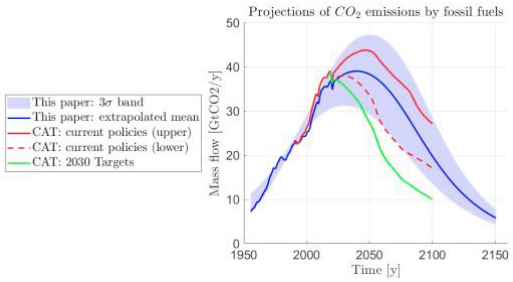

Fig. 5 – This paper and CAT CO_2 emission projections.

The comparison with CAT data is shown in Fig. 5. CAT profiles refer to the CO_2 equivalent emission of the whole GHGs, including methane and nitrous oxide. Overlapping has been improved by downshifting the CAT profiles by the offset $\Delta u \cong 13\ \mathrm{GtCO_2/y}$, which matches the sum of methane and nitrous oxide equivalent emissions. The CAT profiles, in red colour, refer to current policies scenario: The uncertainty band fairly coincides with the paper finite-reserve projections.

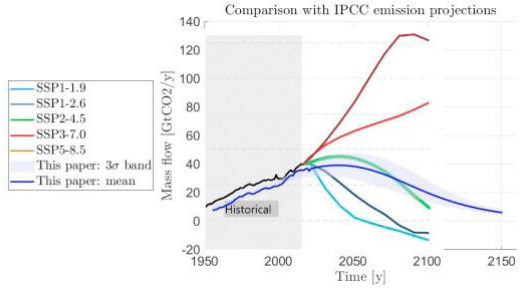

Fig. 6 – CO_2 emission projections: IPCC and this paper.

The comparison with recent IPCC projections is in Fig. 6. In this case, they were untouched since they just refer to CO_2 emissions. The five scenarios are explained in IPCC (2022). SSPx-y.y stands for Shared Socioeconomic Pathway, x=1 to 5 denotes the class and y.y the net radiative forcing [W/m^2] at year 2100. Radiative forcing stands for the algebraic sum of natural and anthropogenic exogenous radiant energy fluxes [W/m^2], which perturb the energy equilibrium of the Earth's biosphere and consequently the climate.

The offset of about 5 $\mathrm{GtCO_2/y}$ between historical data likely amounts to the land-use change emission (u_3 in (6)), whose mean value $\underline{u}_3$, as explained in Section 2.1, contributes to the equilibrium $\underline{x}$ in (8). SSP3-7.0 and SSP5-8.5 projections look fully outside of the envelope of the finite-reserve projections. SSP2-4.5 projection (green, emissions around current levels until 2050, then falling but not reaching zero by 2100) looks close to the mid profile of the CAT projections in Fig. 5, and therefore to the mean finite-reserve projection. A similar conclusion can be found in Ward et al. (2011).

4. AIRBORNE CO_2 CONCENTRATION PROJECTION

Replacement of the input $u(t)$, in equation (8), with the mean and 3σ lower and upper profiles of $c(t) = \sum_{f=1}^{3} c_f(t)$ in Fig. 4 (black line), and integration for $t_0 \le t \le t_{end}$, allows the annual mean airborne CO_2 concentration $x(t)$ to be projected as a balance between the opposite contributions of fossil-fuel emission and land/ocean absorption. The resulting mean profile and the 3σ uncertainty band are reported in Fig. 7. The dashed red line, which overlaps the mean profile until $t_p = 2021$, corresponds to the annual mean of the Mauna Loa data in Fig. 1 (blue). The uncertainty band accounts for the emission band in Fig. 4 and the parameter a posteriori standard deviation in Table 1, last column.

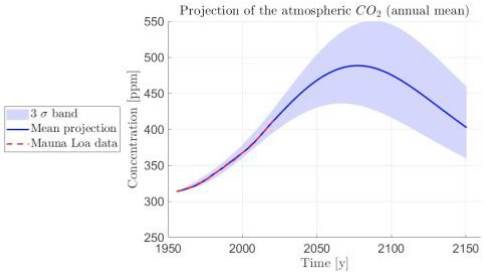

Fig. 7 – Finite-reserve projection of the airborne CO_2 concentration and the Mauna Loa data (dashed red).

The delay $\Delta t_{max} = t_{x,max} - t_{c,max}$ in Table 2 is coherent with τ of equation (8) and Table 1. If a duration $\Delta t_c \cong 220$ y of the total emission wave in Fig. 4 in guessed, we get

$$\Delta t_{max} \cong \frac{\Delta t_c}{2\pi} \tan^{-1}\left(\frac{2\pi\tau}{\Delta t_c}\right) \cong 35\ \text{y}. \qquad (18)$$

Table 2 summarizes the range of the peak dates for both the total projected CO_2 emission by fossil fuels in Fig. 4 and the projected airborne concentration in Fig. 7.

Table 2 – Peak date and range: emission and concentration

No	Variable	Parameter	Symbol	Unit	Range
1	Concentration	Date	$t_{x,max}$	y	2064 ~ 2084
2	Emission	Date	$t_{c,max}$	y	2031 ~ 2047
3	Concentration	Delay	Δt_{max}	y	33 ~ 37

Comparison with IPCC projections is shown in Fig. 8. At first sight, comparison looks coherent with Fig. 5, in the sense that SSP3-7.0 and SSP5-8.5 projections are fully outside of the envelope defined by the finite-reserve projections, and SSP 2-4.5 projection (green colour) drifts away from the mean profile of this paper (blue) because of the offset in Fig. 6.

Actually, the drift deserves insight based on (8) and Table 1. The offset value (between green and blue profiles in Fig. 6) roughly amounts to $\Delta u \simeq \mu_{CO2} 5\ \mathrm{GtCO_2/y} = 0.64\ \mathrm{ppm/y}$ and lasts for about $\Delta t = 100$ y before becoming negative. The

resulting perturbation $\Delta x(t)$ must stay below the steady-state $\Delta x_\infty = \hat{\tau}\Delta u \simeq 26 \sim 42$ ppm. Actually, the overshoot at $t = 2100$ looks larger than 100 ppm. Complex dynamic models like Earth System and General Circulation Models (see Annex II of IPCC, 2022) should be more liable to drift than simpler models. As a hint, overshoots of this kind may be attributed to longer time constants than that estimated in the paper.

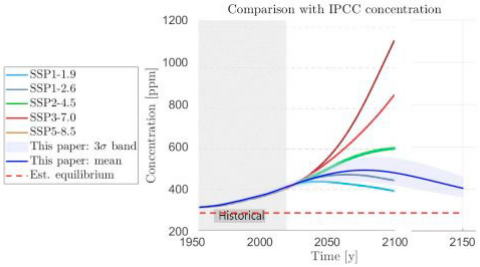

Fig. 8 – Airborne CO_2 concentration: IPCC and this paper.

A rebuttal may address the short interval (1955 to 2021) of the regression measurements, of the same order of $\hat{\tau}$. Firstly, data short-time duration reflects into the estimate uncertainty in Table 1. Secondly, extension to longer past intervals (Mazza, Canuto and Novara, 2022) has shown rather invariant estimates, and, as already cited in Section 2.3, a confirmation can be deduced from Zhang et al, 2021. A further concern may address variability due to ocean and land conditions. The kinetic constant k may include scaled perturbations driven by measurable and predictable exogenous variables.

6. CONCLUSIONS

The paper is driven by two observations: 1) the atmospheric CO_2 growth rate is smaller than that ascribed to the emission of fossil-fuel combustion; 2) fossil-fuel reserves are finite. The first observation leads to a simple state equation capable of accounting for the airborne CO_2 absorption by land and ocean. The second observation leads to a simple logistic curve for forecasting the emission of fossil fuels under reserve constraint. Driving the state equation by the projected emissions allows the airborne concentration to be projected close to the zero-reserve epoch. The resulting profiles may be taken as upper physical limits to other scenarios.

The method is rooted into simple physical differential models, whose parameters can be easily estimated and checked from historical data. Something similar has been done in Zhang et al., 2021, but for static difference equations. The projections of the fossil fuel emissions have been derived by constraining them by proven reserves. Extension to GHG emissions from non-fossil sources was not the aim. Comparison with well-known projections of the airborne CO_2 concentration has aided, with a reasonable confidence, a reciprocal check. As a result, IPCC projections look in some instances incompatible with finite-reserve constraints.

The aims of the future research can be summarized as follows. (i) To include other GHGs emissions, partly constrained by finite reserves, in the future projections. (ii) To identify the proper land and ocean kinetic constants of the complex model in (4), with the help of historical data. (iii) To study and develop control strategies for the energy apportionment, in order to aid a progressively reduction of fossil-fuel combustion under the energy demand.

REFERENCES

Archer D. (2010). *The Global Carbon Cycle*, Princeton University Press, Princeton, NJ.

Bebbington J. et al., (2020). Fossil-fuel reserves and resources reporting and unburnable carbon: Investigating conflicting accounts, *Critical Perspectives on Accounting,* 66, 1-22.

Climate Action Tracker (2022). *Global temperatures addressing global warming,* at https://climateactiontracker.org/global/temperatures/.

Connolly et al. (2020). How much human-caused global warming should we expect with business-as-usual (BAU) climate policies? A semi-empirical assessment. *Energies,* 13 (8).

Eyring V. et al. (2016), "Overview of the couple model intercomparison project phase 6 (CMIP6) experimental design and organization", *Geosci. Model Development*, 9, 1937-1958.

Friedlingstein P. et al. (2003), How positive is the feedback between climate change and the carbon cycle? *Tellus B, Chemical and Physical Meteorology,* 55 (2), 692-700.

Friedlingstein P. et al. (2022), Global Carbon Budget 2021, *Earth Syst. Sci. Data*, 14.

Houghton J.T. et al. (1990), *Climate Change, The IPCC scientific assessment*, Cambridge Univ. Press, Cambridge, UK

IPCC (2021), Climate Change 2021: The Physical Science Basis, in Masson-Delmotte V. et al. eds., *Contribution of Working Group I to the Sixth Assessment Report of the IPCC*, Cambridge University Press, Cambridge, UK.

IPCC (2022), Summary for Policymakers, in Shukla P.R. et al. eds, *Climate Change 2022: Mitigation of Climate Change*, Cambridge University Press, Cambridge, UK.

Lindsay R. (2022). *Climate change. Atmospheric carbon dioxide,* at https://www.climate.gov/news-features/understanding-climate/climate-change-atmospheric-carbon-dioxide.

Mazza D. and Canuto E. (2022). *Fundamental Chemistry with Matlab,* Elsevier, Amsterdam, The Netherlands.

Mazza D., Canuto E. and Novara C. (2022). Depletion of fossil fuel reserves and projections of CO2 concentration in the Earth's atmosphere, submitted to *Environm. Modeling and Assessment.*

Peng S. et al. (2022), Wetland emission and atmospheric sink changes explain methane growth in 2020, *Nature,* 612, 477-482.

Regnier P. et al. (2022), The land-to-ocean loops of the global carbon cycle, *Nature,* 603, 402-410.

Revelle R. and Suess H.E. (1957). Carbon dioxide exchange between atmosphere and ocean and the question of an increase of atmospheric CO_2 during the past decades, *Tellus,* 9 (1), 18-27.

SCRIPPS CO_2 Program (2022), *Atmospheric CO_2 Data, Ice-core Merged Products,* dataset from https://scrippsco2.ucsd.edu/data/atmospheric_co2/icecore_merged_products.

Tans P. (2009). An accounting of the observed increase in oceanic and atmospheric CO_2 and an outlook for the future, *Oceanography,* 22 (6), 26-35.

Vernon C. et al. (2011). Carbon dioxide emission scenario: limitations of the fossil fuel resource, *Proc. Environment Sciences*, 64, 206–215.

Ward J.D. et al. (2011). The influence of constrained fossil fuel emissions scenarios in climate and water resource projections, *Hydrology and Earth Systems Science*, 15, 1879-1893.

Welsby D. et al. (2021). Unextractable fossil fuels in a 1.5°C world, *Nature*, 597, 230-234.

Zhang X. et al. (2021), A small climate- amplifying effect of climate-carbon cycle feedback, *Nature Communications,* Vol. 12, paper 2952 (2021), pp.1-11.

Zeebe R.E and Wolf-Glabrow D. (2001). *CO2 in Seawater: Equilibrium, Kinetics, Isotopes.* Elsevier, Amsterdam.